8

Peculiarity of the Cathodoluminescence of Alpha- Alumina Prepared by Calcination of Gibbsite Powder or Generated by Oxidation of a Metallic FeCrAl Alloy

Djelloul Abdelkader and Boumaza Abdecharif
Laboratoire des Structures, Propriétés et Interactions Inter Atomiques (LASPI²A)
Centre Universitaire de Khenchela 40000
Algeria

1. Introduction

Most of metallic materials functioning at high temperature need to have oxidation resistance. This resistance can be achieved when the material develops, through oxidation, an oxide film which acts as a diffusion barrier while keeping a good adherence. In this respect, alpha alumina clearly acts as such. The oxides of aluminum have been the subject of many investigations because of their commercial importance and scientific interest. The thermal stability and optical properties of pure nanometer-sized alumina powder have received much attention because of their intrinsic interest and commercial value. Nanometer-sized alumina powders are widely applied today. One of its applications is in fluorescent lamps due to the absorption of ultraviolet light. In fact, it can also emit the light under excitation with a suitable wavelength. It is important to note that there are many works about alpha alumina using X-ray diffraction, but there is a need for a more detailed structural analysis. To achieve this more exhaustive structural characterization we have used the Rietveld refinement method and cathodoluminescence (CL) measurements.

CL spectroscopy is widely used as a contactless and relatively nondestructive method to provide microcharacterization of the optical and electronic properties of luminescent materials. Nevertheless, it is used comparatively rarely for the investigation of oxide semiconductor structures. The major advantage of CL spectroscopy in the case of such structures is that most of the anticipated products of oxidation are luminescent, and it is easy to get excitation across the bandgap of any dielectric with readily available electron beam voltages. The emission occurs for all the luminescent mechanisms present in the material.

Pure α-Al_2O_3 crystal is colorless and shows little absorption in the ultraviolet–visible (UV–Vis) range. But various impurities (Ti, Mn, Cr, and Fe) even a trace level causes apparent absorptions which are attributed to various emission centers (Jheeta et al., 2006).

The colors arise from very minor amounts of impurity (<1% of the Al^{3+} replaced by other cations) because the Al_2O_3 structure apparently does not tolerate substitutions. However,

these trace substitutions can cause intense colors. Ruby is red because of its Cr^{3+} content. Yellow sapphire owes its color to Fe^{3+}. Blue sapphire derives its color from Fe^{2+}-Ti^{4+} and Fe^{2+}-Fe^{3+} intervalence charge transfer. Green sapphires contain a mixture of the blue and green colors.

Strong well-known $^2E \rightarrow {}^4A_2$ lines of Cr^{3+} (693 nm) with a long decay time characterize their luminescence spectra. Besides that, much weaker narrow lines are present, which are connected with Cr-pairs and more complicated complexes. The Mn^{4+} ion is isoelectronic with Cr^{3+}, i.e., both of them have the same electronic structure of the open shell ($3d^3$ configuration). Thus, the spectroscopic properties of α-Al_2O_3:Mn^{4+} are similar to those of ruby (α-Al_2O_3:Cr^{3+}). Octahedral Mn^{4+} ($3d^3$) would be expected to show the R-line fluorescence characteristic of isoelectronic Cr^{3+} and in approximately the same region. The dominate defects for the visible emission might be different for α-alumina powders formed by heating any of the hydrates of aluminium to a sufficiently high temperature.

In the presence of lattice defects, extra luminescence emissions can be observed in the ultra-violet (UV) region upon highly energetic excitation. The main intrinsic defects in the α-alumina crystals are oxygen vacancies in different charge states: a neutral vacancy, a vacancy capturing one electron (a F^+-center), and a vacancy capturing two electrons (a F-center) (Kislov et al., 2004; Michizono et al., 2007; Yu et al., 2002). The observed UV spectrum in α- alumina can be deconvoluted into two distinct sub-band components: an F^+-center band, located at around 3.8 eV, and a less intense F-center band, located at around 3.0 eV (Brewer et al., 1980; Boumaza & Djelloul, 2010; Boumaza et al., 2010). Depending on the defect introduction method one can create also F_2-centers, F_2^+-centers and F_2^{2+}-centers (double oxygen vacancy with four, three and two trapped electrons respectively). α-Al_2O_3 crystals with defects in the oxygen sublattice are actively studied as promising storage materials (Kortov & Milman, 1996). In this connection, it is interesting to study luminescence properties of the nanostructured aluminium oxide and compare them with analogous properties of crystalline samples.

In this chapter, we present X-ray diffraction (Rietveld analysis) and CL measurements of α-alumina powders formed by calcination of gibbsite or generated by oxidation of a metallic FeCrAl alloy. The peculiarity of the cathodoluminescence under comparable conditions of α- alumina is discussed.

2. Materials and experimental methods

Gibbsite powder, $Al_2(OH)_6$, from Prolabo (no 20 984.298) was used. The powder is made of platelet aggregates and was composed of 64.5–67% Al_2O_3 and max.: 0.01% Fe_2O_3, 0.02% SO_4, 0.002% heavy metals (as Pb), and 1.0% non precipitable by NH_4OH (as SO_4). The sample experienced an ignition loss of 33–34.5% at 1000 °C and had a purity grade of 99.7%. Its average particle size (20 μm) was due to the agglomeration of crystallites. The specific surface area of the original sample was 0.5 m^2/g.

The gibbsite platelets was calcined in ambient atmosphere (pO_2 = 0.21 atm) at 1573 K. The cycle was as follows: heating up to an isothermal temperature at 5 K/min, maintaining for 24h at the calcination temperature and fast cooling down to room temperature (air quench). The calcination temperature was maintained for 24 hours to obtain a well-crystallised product.

The present work was performed on ferritic ODS commercial FeCrAlY alloy PM2000 (20 wt% Cr, 5.8 wt% Al, 0.5 wt% Ti, 0.5 wt% Y_2O_3). This alloy is an alumina-forming alloy. The specimens, with dimensions 25×25×5 mm^3, are cut from a rolled plate. In the case of the PM2000, sample was oxidised in air at 1223 K for 72h. The thermogravimetric method (TG) and differential thermal analysis (DTA) data were recorded under a dry air flow with a heating rate of 10 K/min in a SETARAM TGDTA92–16.18 thermal analyser. TG measurements were corrected for temperature–dependent buoyancy by subtracting the data of a measurement carried out on an inert sample. The crystalline structure of the sample was investigated by XRD using a PANalytical X'Pert Pro MRD diffractometer configured as follows: Cu tube operating at 40 kV and 30 mA ($\lambda(Ka_1)$ = 0.15406 nm, $\lambda(Ka_2)$ = 0.15444 nm). The scan rate (2θ) was 1°/min at a step size of 0.025°. The data were processed to realize the conditions of the software program Fullprof Suite for the structure refinement.

The FTIR technique was used in the absorbance mode in the 200-4000 cm^{-1} range. For oxides all bands have characteristic frequencies between 200 and 1000 cm^{-1}. For the FTIR measurements, samples were prepared by grinding the oxide films scraped from the substrate (PM2000). After calcination, 10 to 100 µg of the powder was drawn, then grinded with 23 ±2 mg of CsBr in order to obtain, a pellet of 200-250 µm in thickness. After grinding, the powder was placed in a mould (5 mm diameter) and a cold isostatic pressure (CIP) of 150 MPa was applied for 5 min.

The FTIR spectra are obtained using a Perkin-Elmer spectrometer at resolution of 8 cm^{-1}. For each sample, 120 scans were used. The apparatus is equipped with a system allowing the reduction of the optical course in air in order to minimize the perturbations associated with ambient air (water vapour and CO_2). The uncertainty on the position of the various peaks is equal to ± 2 cm^{-1}.

The emitted light under electron beam excitation in a UHV system was analyzed through a quartz window with a Jobin Yvon CP 2000 spectrograph and a CCD detector. The wavelength range 200-1000 nm was investigated.

3. Results and discussions

3.1 Differential thermal analysis and thermal gravimetry analysis (DTA-TG) of gibbsite

Fig. 1 shows the typical TG–DTA curves of the gibbsite. TG and DTA curves are indicated as dotted and solid lines, respectively. Concerning the dehydration-dehydroxylation process of gibbsite, the dehydration appears to occur in two steps (around 598 and 803 K respectively) at higher temperature. The expected theoretical loss due to dehydration is 34.6%, the experimental loss is 34.3% a little lower. This difference 0.3% is a bit larger than the experimental uncertainty 0.1%, the starting gibbsite may be slightly dehydrated. The last step (803 to 1273 K) gives no thermal event but appears as a continuous mass loss (about 2%) which corresponds to the elimination of residual hydroxyls. The formation of α–alumina occurs between 1473 and 1533 K (MacKenzie et al., 1999). Finally, the structural transformations to well-crystallised α−alumina are described by nucleation (T<1470 K) and growth mechanisms (T>1470 K).

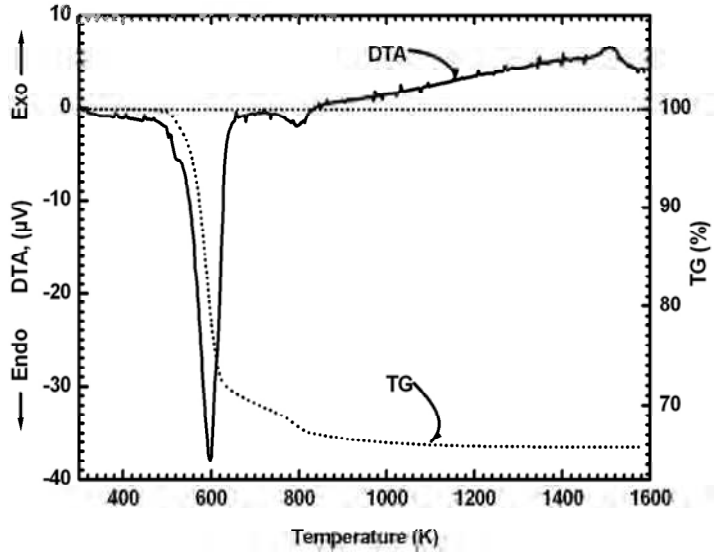

Fig. 1. TG and DTA curves of gibbsite.

3.2 Gibbsite

Gibbsite (γ-$Al(OH)_3$) has monoclinic symmetry (a=0.8684, b=0.5078, c=0.9736 nm, β=94.54°) with the space group P21/n, and the unit cell contains eight $Al(OH)_3$ units (Saalfeld & Wedde, 1974). Gibbsite is characterized by the stacking of two-layer units (AA or BB) of hydroxyl sheets with the sequence ABBAABBA... where hydroxyl sheets of the adjacent Gibbsite layers face the c direction (Kogure, 1999). In Fig. 2a, the XRD pattern obtained on the as received gibbsite powder shows a good agreement with the reference XRD pattern (33-0018 JCPDS file).

3.2.1 Phase transitions induced by heat treatment of gibbsite

When heating up fine-grained gibbsite, most OH groups are eliminated, and various forms of alumina are formed with the sequence: gibbsite →χ-→κ-→α-Al_2O_3 when temperature increases. In order to study these phases, we performed XRD measurements on four samples prepared from gibbsite calcined for 24h at 773, 1073 (62h), 1173 and 1573K respectively.

According to Fig. 2b, at 773K ,the χ phase is expected. In spite of many investigations since the1950's (Brindley & Choe, 1961; Kogure, 1999; Saalfeld, 1960; Stumpf et al., 1950; Yu et al., 2002), the crystal structure of χ-alumina is still uncertain. Stumpth et al. (Stumpf et al., 1950) assumed a cubic (not spinel) unit cell of lattice parameter a=0.795 nm (04-0880 JCPDS file). On the other hand, two hexagonal structures have been suggested, either with the parameters a=0.556 nm and c=1.344 nm (Saalfeld, 1960) or with a=0.557 nm and c=0.864 nm (Brindley & Choe, 1961) (13-0373 JCPDS file). The two previous hexagonal unit cells may be described respectively as a stacking of 6 and 4 close-packed oxygen layers, of approximately the same thickness (0.224 and 0.216 nm) as the Al–OH layers in gibbsite (0.212 nm). More

recently, Kogure (Kogure, 1999) proposed a hexagonal lattice with a=0.49 nm and an undefined c length indicating that χ-alumina structure can be regarded as random close packing of gibbsite-like layers.

For samples prepared at 1173 K, the κ phase is expected (see Fig. 2d). Contrary to the χ phase, the crystal structure of κ-alumina is well known (see for example Ref. (Ollivier et al., 1997) and references therein). κ-alumina is orthorhombic with the space group $pna2_1$ and results in ten independent atoms positions (four Al and six O). The experimental XRD pattern at 1173K is specific of a pure κ-alumina (Fig. 2d). Nevertheless, the presence of remnant χ-phase cannot be excluded as all the χ peaks also appear in κ structure. Note that the experimental XRD patterns show well crystallized phases, in contrast with the χ phase.

Fig. 3 give SEM images and XRD patterns of gibbsite powder (a) after calcination at (b)- 773 K; (c)- 1073 K; (d)- 1573 K, for 24 h.

When heating up at temperature above 1573K for 24h, gibbsite transforms into α-alumina, the stable structure. The XRD pattern of the 1573K sample (Fig. 6) shows that only α-Al_2O_3 is present when compared with 42–1468 JCPDS file. In this structure, tetrahedral Al^{3+} ions are no longer present and only AlO_6 octahedron remain.

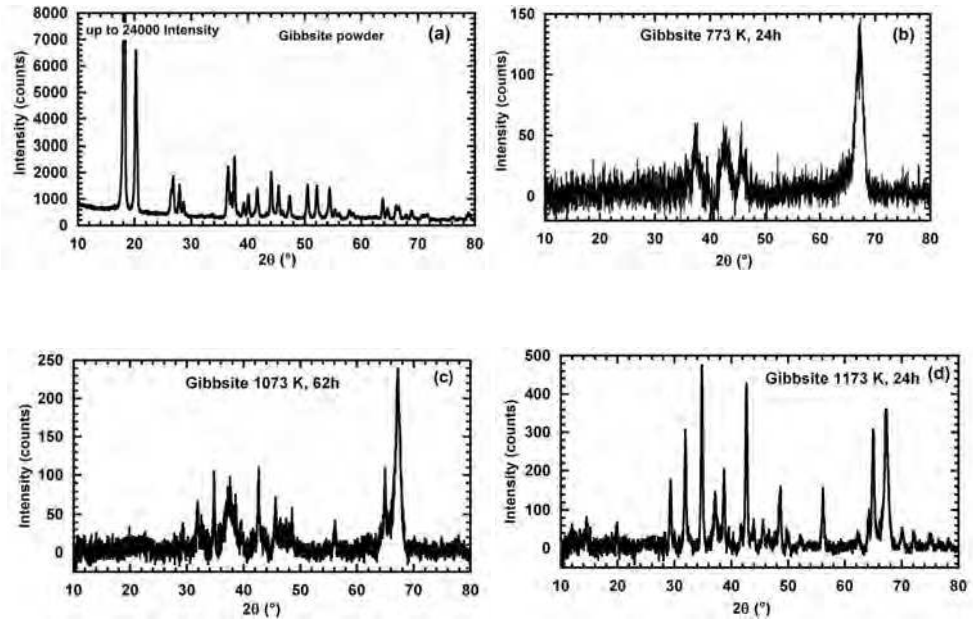

Fig. 2. XRD patterns: (a) Gibbsite (33-0018 JCPDS file), (b) alumina formed from gibbsite calcined for 24h at 773K (expected χ phase) (JCPDS 13-0373 file), (c) alumina formed from gibbsite calcined for 62h at 1073K, (d) alumina formed from gibbsite calcined for 24h at 1173K (expected κ phase) (JCPDS 88-0107 and 01-1305 file).

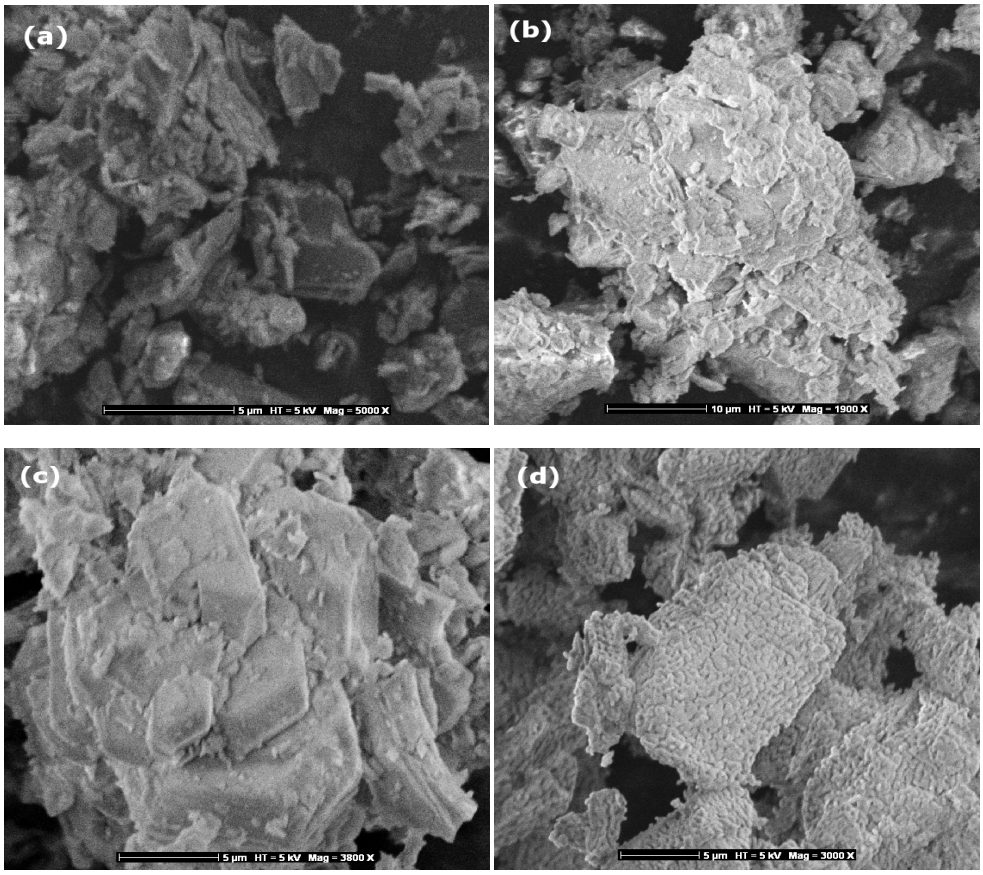

Fig. 3. SEM images: (a)- Gibbsite; (b)- 773 K; (c)- 1073 K; (d)- 1573 K.

3.2.2 General properties of alumina (Al_2O_3)

Aluminum oxide, commonly referred to as alumina, possesses strong ionic interatomic bonding giving rise to it's desirable material characteristics. It can exist in several crystalline phases which all revert to the most stable hexagonal alpha phase at elevated temperatures. This is the phase of particular interest for structural applications and the material available from Accuratus.

The exceptional properties of alumina (Al_2O_3), such as great hardness, high thermal and chemical stability, and high melting temperature, make it a very attractive material. The crystalline α-Al_2O_3 phase (corundum or sapphire) is the single stable modification of alumina. The crystalline α-Al_2O_3 has the band gap Eg≈8.5 eV and is widely used in optical devices. Sapphire doped with chrome (ruby) or titanium is applied as an active medium in laser systems. In microelectronics sapphire is used as a substrate for growing silicon and gallium nitride (GaN). Alumina is a highly radiation-resistant material and is used as a sensitive element in detectors when measuring the ionizing radiation parameters.

High purity alumina is usable in both oxidizing and reducing atmospheres to 1925°C. Weight loss in vacuum ranges from 10^{-7} to 10^{-6} g/cm².sec over a temperature range of 1700° to 2000°C. It resists attack by all gases except wet fluorine and is resistant to all common reagents except hydrofluoric acid and phosphoric acid. Elevated temperature attack occurs in the presence of alkali metal vapors particularly at lower purity levels.

The composition of the ceramic body can be changed to enhance particular desirable material characteristics. An example would be additions of chrome oxide or manganese oxide to improve hardness and change color. Other additions can be made to improve the ease and consistency of metal films fired to the ceramic for subsequent brazed and soldered assembly.

Mechanical, thermal and electrical properties of Al_2O_3 are summarized in table 1.

	Units of Measure	**94% Al_2O_3**	**96% Al_2O_3**	**99.5% Al_2O_3**
Mechanical				
Density	gm/cc	3.69	3.72	3.89
Porosity	%	0	0	0
Color	—	white	white	ivory
Flexural Strength	MPa	330	345	379
Elastic Modulus	GPa	300	300	375
Shear Modulus	GPa	124	124	152
Bulk Modulus	GPa	165	172	228
Poisson's Ratio	—	0.21	0.21	0.22
Compressive Strength	MPa	2100	2100	2600
Hardness	Kg/mm²	1175	1100	1440
Fracture Toughness K_{IC}	MPa•m$^{1/2}$	3.5	3.5	4
Maximum Use Temperature	°C	1700	1700	1750
Thermal				
Thermal Conductivity	W/m•K	18	25	35
Coefficient of Thermal Expansion	10^{-6}/°C	8.1	8.2	8.4
Specific Heat	J/Kg•K	880	880	880
Electrical				
Dielectric Strength	ac-kV/mm	16.7	14.6	16.9
Dielectric Constant	At 25°C, 1 MHz	9.1	9.0	9.8
Dissipation Factor	At 25°C, 1 MHz	0.0007	0.0011	0.0002
Volume Resistivity	Ohm•cm	>10^{14}	>10^{14}	>10^{14}

Table 1. Mechanical, thermal and electrical properties of Al_2O_3 (http://accuratus.com/alumox.html).

3.2.3 Oxidation of PM2000

The oxidation resistance of high-temperature alloys and metallic coatings is dependent on the formation of a protective surface oxide. In an ideal case, the oxide layer should be highly stable, continuous, slow growing, free from cracks or pores, adherent and coherent. α-Al_2O_3 is an oxide which comes close to satisfying these requirements; the slow growth rate is related to its highly stoichiometric structure and its large band gap which makes electronic conduction difficult.

One of the most crucial factors in the oxidation of alumina-formers is the temperature, which must be high enough to promote the formation of α-Al_2O_3 in preference to the less protective transition alumina. Another critical factor is the aluminum content which must be sufficiently high to develop and maintain an alumina layer and prevent subsequent breakaway oxidation.

The addition of chromium to Fe-Al alloys promotes the formation and maintenance of a complete layer of α-Al_2O_3 by acting as a getter and preventing internal oxidation of the aluminum (Wood, 1970).

Iron and chromium are the major impurities present in Al_2O_3 scales formed on PM2000. Primarily their oxides formed during the transient stage and were incorporated into the α-Al_2O_3 scale. Fe segregated to some α-Al_2O_3 grain boundaries, but not Cr. The Al_2O_3 scale became progressively purer with oxidation time. It is possible that the Fe in the Al_2O_3 scale increases the scaling rate and, in particular, enhances lateral growth that causes scale convolution.

The growth of α-Al_2O_3 scales that form on FeCrAl alloys during high temperature oxidation is generally considered to be controlled by oxygen inward diffusion through oxide grain boundaries (Mennicke et al., 1998; Quaddakkers et al., 1991). Aluminum also diffuses out, which can cause growth within the scale (Golightly et al., 1979). The degree of Al outward transport can be significantly reduced by the presence of reactive elements, such as Y, Hf or Zr (Mennicke et al., 1998; Quaddakkers et al., 1991), which segregate to Al_2O_3 grain boundaries (Przybylski et al., 1987). However, the extent of outward growth seems to differ appreciably among several reactive-element doped Fe based alloys.

The EDS results of the average Fe and Cr concentrations in the scale as a function of scale thickness from different transmission electron microscopy (TEM) specimens are summarized in Table 2.

Oxidation condition	Scale thickness (μm)	Oxide grain size (nm)	Average [Cr] (at%)	Average [Fe] (at%)	Lattice parameter (nm)
1000 °C, 0.5 h	0.39	107±36	4.12±0.95	4.49±1.67	a = 0.495±0.004 c = 1.353 ± 0.008
1000 °C, 1 h	0.9	191±44	0.34±0.28	1.91±0.49	a = 0.475±0.004
1000 °C, 26 h	1.77	186±53	0.24±0.28	0.60±0.32	c = 1.347 ± 0.008
1200 °C, 2 h	2.94	291±46	0.3±0.64	0.70±0.57	a = 0.471±0.004
1200 °C, 120 h	4-5.5	1546±423	0.27±0.20	0.06±0.06	c = 1.323 ± 0.008

Standard parameters for α-Al_2O_3 are: a = 0.4758 nm, c = 1.2991 nm.

Table 2. Fe and Cr concentrations in α-Al_2O_3 scales and effect on lattice parameters (Hou et al., 2004)

Fig. 4 give SEM images and XRD patterns of PM2000 after oxidation at 1023 K for 76 h and 1223 K for 72 h.

EDX analysis (Fig. 5) of the sample oxidized at 1123 K indicates that the film mainly consists in aluminium and oxygen elements and very small amount of the substrate constituting elements are observed. As the film thickness decreases, like sample oxidized at 1023 K, the signature of the substrate increases due to interactions of the electrons with the underlying substrate mater as the film is thinner than that formed at 1123 K.

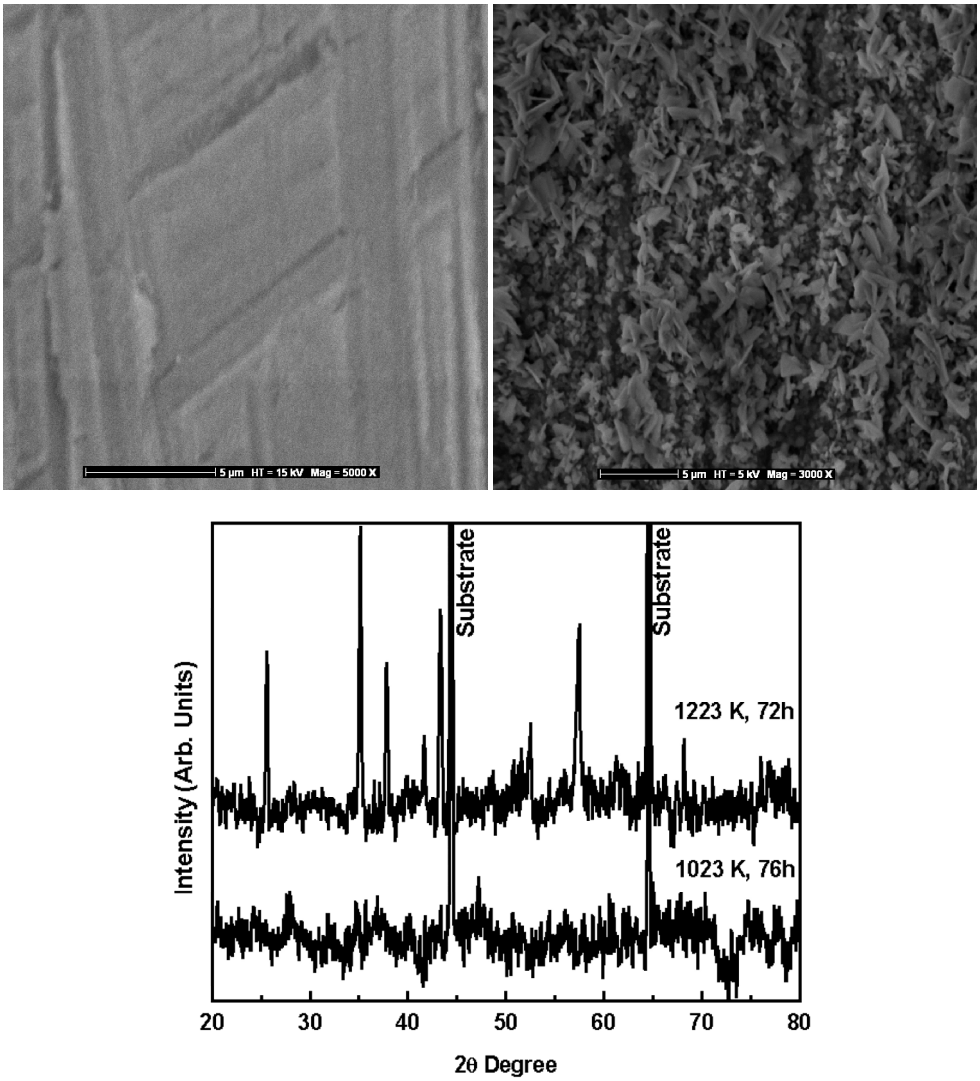

Fig. 4. SEM images of the outer oxidized surface and XRD patterns of α-Al_2O_3 obtained by oxidation of PM2000 at 1023 K for 76 h and 1223 K for 72 h.

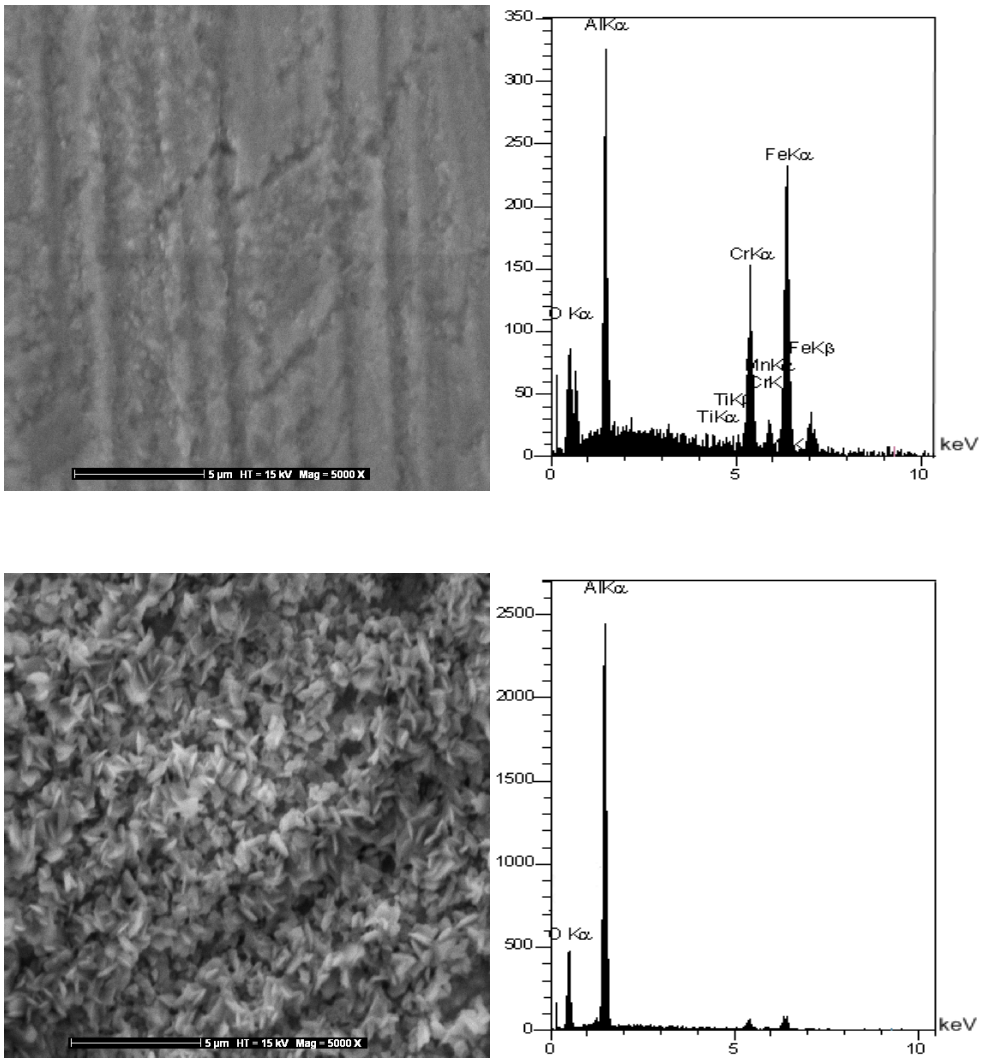

Fig. 5. SEM images of the outer surface and EDX analyses of α-Al_2O_3 films obtained by oxidation of PM2000 in air at 1023 K for 76 h (top) and 1123 K for 95 h (bottom).

3.2.4 Rietveld refinement of the structures

The Rietveld refinement of the structures was performed using the WinPlotr/FullProf suite package (Rodríguez-Carvajal, 1993). The peak shape was described by a pseudo-Voigt function, and the background level was modeled using a polynomial function. The profiles were refined using the space group and structure models of Al_2O_3 ($R\bar{3}C$, JCPDS 46-1212) (in this structure cations occupy the 12c sites and oxygen ions the 18e sites).

The XRD data for the 2θ regions between 20° and 80° was used for the refinement. The observed, Rietveld refined and difference patterns are shown in Figs. 6 and 7.

It was obvious that the agreement between the experimental data and the simulations was excellent since the R_{wp} (weighted residual error) factor was small (≤ 14.1%). The Rietveld results (cell parameters, atom position, reliability factors and crystallite size (D)) are given in Table 3 and 4. The size of α-alumina crystallites (D=36 nm) obtained using PM2000 alloy was smaller than that (D=43 nm) obtained using gibbsite precursor. Furthermore, the α-Al_2O_3 from PM2000 has a greater lattice parameter (a=0.4763nm, c=1.3047nm) than that of JCPDS file 46-1212 (a=0.4758 nm, c=1.2991 nm, c/a=2.730) and a greater c/a ratio (c/a =2.739) than that of JCPDS file 46-1212. However, the α-Al_2O_3 from gibbsite has a smaller lattice parameter (a=0.4752nm, c=1.2980nm) and a similar c/a ratio (c/a =2.731) than that of JCPDS file 46-1212. Furthermore, the α-Al_2O_3 from gibbsite has a greater calculated density (3.996 g/cm^3) than that of α-Al_2O_3 from PM2000 (3.961 g/cm^3). Phase transformations are frequently accompanied by microstructural changes. This fact could explain the crystallographic parameters differences between a two α-alumina.

Lattice parameters (nm)	atom	Wyck.	Site	x	y	z	Biso	occupancy
a= 0.47523 c= 1.29805	**Al**	12c	3.	0	0	0.3521	0.2200	0.3333
	O	18e	.2	0.3065	0	0.2500	0.2400	0.5000

Table 3. The Rietveld refinement results: α-Al_2O_3 from gibbsite powder, R_p= 16.7%, R_{wp}= 6.93%, Calc. density =3.996 g/cm^3, D=43 nm.

Lattice parameters (nm)	atom	Wyck.	Site	x	y	z	Biso	occupancy
a= 0.47637 c= 1.30472	**Al**	12c	3.	0	0	0.3417	4.7208	0.9602
	O	18e	.2	0.3392	0	0.2500	2.7191	1.1186

Table 4. The Rietveld refinement results: α-Al_2O_3 from PM2000, R_{wp}= 14.1%, Calc. density =3.961 g/cm^3, D=36nm.

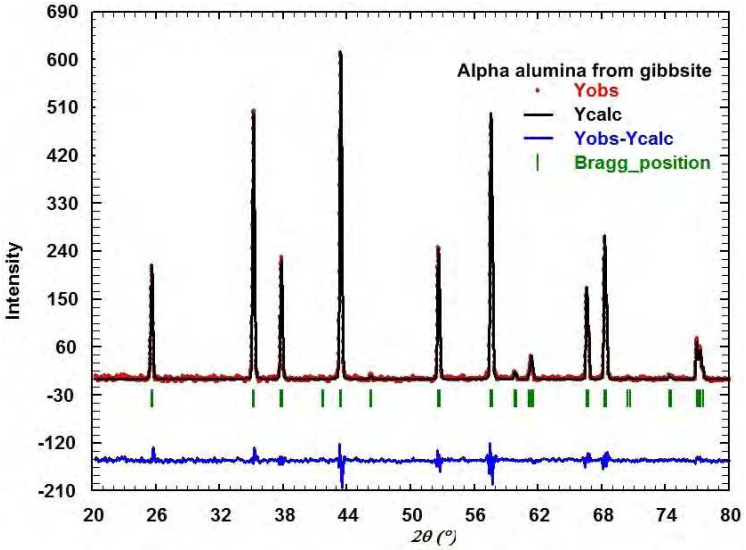

Fig. 6. The observed and calculated diffraction patterns of α-alumina powder prepared by calcination at 1573K for 24h of gibbsite powder. Vertical bars indicate the calculated position of the Bragg peaks. The blue curves in the bottom correspond to the differences between experimental and calculated profiles.

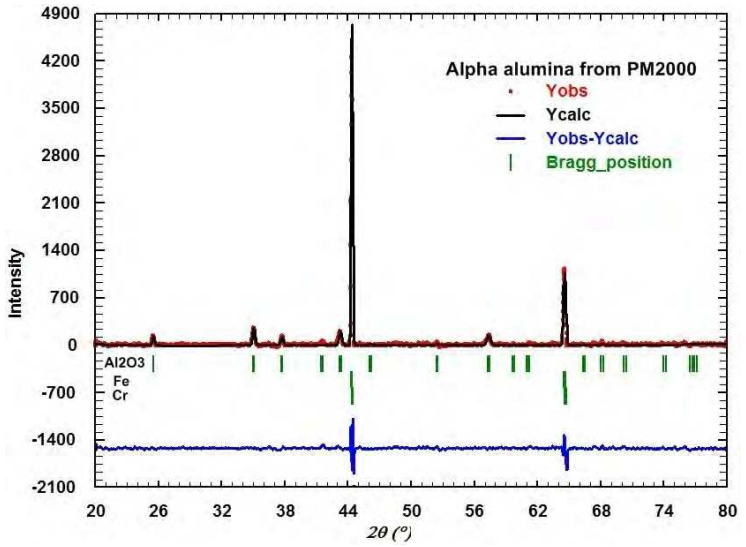

Fig. 7. The observed and calculated diffraction patterns of α-alumina obtained by oxidation of PM2000 at 1223K for 72h.

3.2.5 Fourier transform infrared (FTIR) analysis

Fig. 8 compares the FTIR absorbance spectra of α–Al_2O_3 obtained after calcination of gibbsite and oxidation of PM2000. For the samples calcined at 1573 K, significant spectroscopic bands at ~640, ~594, ~447 cm^{-1} and ~386 cm^{-1} appear which are identified to be the characteristic absorption bands of α-Al_2O_3 (Barker, 1963). This is in good agreement with XRD observations. Common bands exist in all cases, such as the broad OH band centered around 3420 cm^{-1}, and the 1640 cm^{-1} H_2O vibration band (Ma et al., 2008). The very high surface area of these materials results in rapid adsorption of water from the atmosphere because the FTIR samples were kept and grinded in air. Three peaks of very weak intensities at 2850 cm^{-1}, 2920 cm^{-1} and 2960 cm^{-1} are observed which are due to C-H stretching vibrations of alkane groups. The absorption in ~2356 cm^{-1} is due to CO_2 molecular presence in air.

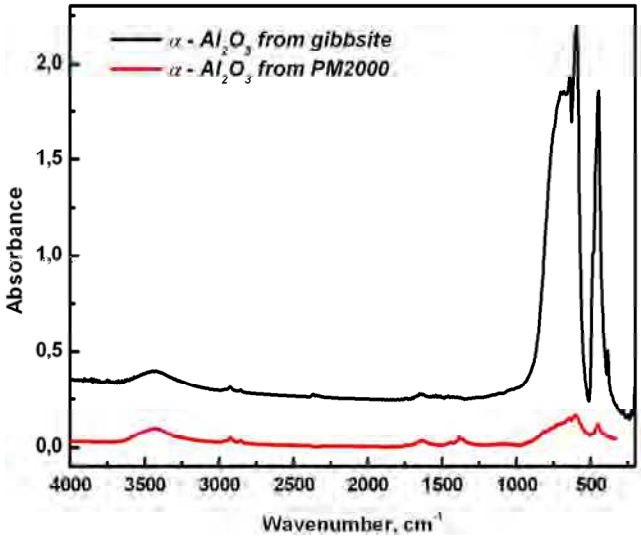

Fig. 8. FTIR absorption spectra of α-alumina powder prepared by calcination of gibbsite (black line) or generated by oxidation of PM2000 (red line).

3.3 Cathodoluminescence

CL is the phenomenon of light emission from specimens as a result of interaction with an electron beam. In insulating crystals, the origin of the luminescence arises from impurity atoms (e.g. transition metals or rare earths) in the crystal lattice. Using an electron microscope to produce the electron beam, the spatial distribution of luminescent sites can be observed with submicron spatial resolution, and correlated with features of the specimen morphology or microstructure.

The mechanisms for CL are similar to those for photoluminescence, but the energy input or excitation source is that of an electron beam rather than a visible or ultraviolet light beam. When an energetic (keV range) electron beam propagates within a semiconductor or insulator, the primary electrons lose energy by the creation of electron-hole pairs. These

electron-hole pairs then recombine via radiative and non-radiative processes. Only the radiative recombination process which leads to the creation of a photon is viewed with CL. Radiative recombination may be intrinsic (arising from electronic states of the perfect crystal) or extrinsic (arising from electronic states that are localized at defects or impurities in the crystal). Extrinsic luminescence thus provides information about defects and impurities in the crystal lattice. For conciseness, the defects and impurities that give rise to extrinsic luminescence are often denoted the luminescence centers. Each type of luminescence center in a particular crystal has a characteristic emission spectrum. The spectrum may contain both narrow lines and broad bands, depending on the energy level structure of the luminescence center and the coupling of the center to the host lattice. CL is advantageous compared to photoluminescence. CL can potentially give additional information about local positions in the sample because the electron beam can be focused on several nanometers. In addition, the CL system operates under UHV conditions of less than 10^{-9} Torr. Hence, CL measurements can be performed in a contamination-free environment, which is very effective in detecting weak luminescence. Moreover, the depth dependent emission profiles can be examined in CL by controlling the accelerating voltage.

3.3.1 Oxygen vacancy in Al_2O_3

CL signal is a good signature of the material qualities and is used in this study to characterize the point defects associated to oxygen vacancies in α-Al_2O_3. The CL spectra of α-Al_2O_3 formed from gibbsite and PM2000 are given in figure 9 and 12.

In figure 9, the CL spectra shows that wide band over the interval of (200–600 nm) consists of a series of overlapping bands. The main emission bands located at about 250 nm (4.96 eV), 281 nm (4.41 eV), 325 nm (3.81eV), 373 nm (3.32 eV) and 487 nm (2.54 eV) occur in alpha alumina powder and also in alpha alumina films generated by oxidation of a metallic FeCrAl alloy**.** We believe that the observed CL peak at 4.96 eV is related to the interband transitions or to defect that is different in origin to the F or F^+ centers in α-alumina. The luminescence band at 4.41 eV is detected only if the excitation density is high and was previously observed in α-alumina by Kortov et al. (Kortov et al., 2008).

In α-Al_2O_3 (corundum structure) each O atom is surrounded by four Al atoms forming two kinds of Al-O bonds of length 0.186 and 0.197 nm. This is why in corundum F-type centers have low C_2 symmetry. Besides, an O vacancy has two nearest neighbor O atoms, forming the basic O triangle with O-O band length of 0.249 nm in perfect corundum. Thus, the F-type centers are surrounded by six nearest atoms which determine mainly their optical properties.

Defects induced in Al_2O_3 may be of various kinds: F centers (oxygen vacancy with two electron), F^+ centers (oxygen vacancy with one electron), F_2 centers (two oxygen vacancies with four trapped electrons), F_2^+ centers (two oxygen vacancies with three electrons) and F_2^{2+} centers (two oxygen vacancies with two electrons) (Ghamdi & Townsend, 1990).

In the case of α-alumina and sapphire, there have been reported a number of F-type centers including the F^+ and F centers (Evans, 1995). As for the luminescence of irradiation defects, it is known that the luminescence of the F^+ center is observed at the UV region around 3.8

eV (325 nm) while that of the F centers is observed at a lower photon energy region around 3.0 eV (410 nm). Thus the presently observed luminescence from α-alumina and sapphire which is centered at 330 and 420 nm can be attributed to the F^+ and F centers. As for the others, it is noted that the luminescence at 250 and 290 nm is also observed in the case of α-alumina. The luminescence intensity at these bands was found to be sensitive to thermal annealing at higher temperatures, and then might be attributed to the effect of some impurities such as OH.

In Ref. (Oster & Weise, 1994), the absorption bands of 220 and 260 nm in pure α-Al_2O_3 crystals have been attributed to F+ absorption bands. Due to the presence of C_2-symmetry in the F^+-center (oxygen vacancy occupied by a single electron) in pure α-Al_2O_3 crystals, the excited state is split into three levels, ^1B, ^2A, and ^2B, according to the theory of La et al. (La et al., 1973), giving three polarized optical absorption bands located at 255, 229 and 200 nm.

The optical properties of these luminescent centres are well known. They possess absorption and emission bands which are produced in the gap as summarised in Fig. 10. F+ centre is characterised by three absorption bands at 6.3, 5.4 and 4.8 eV and emits at 3.8 eV (330 nm). F centre absorbs at 6 eV and emits at 3 eV (415 nm).

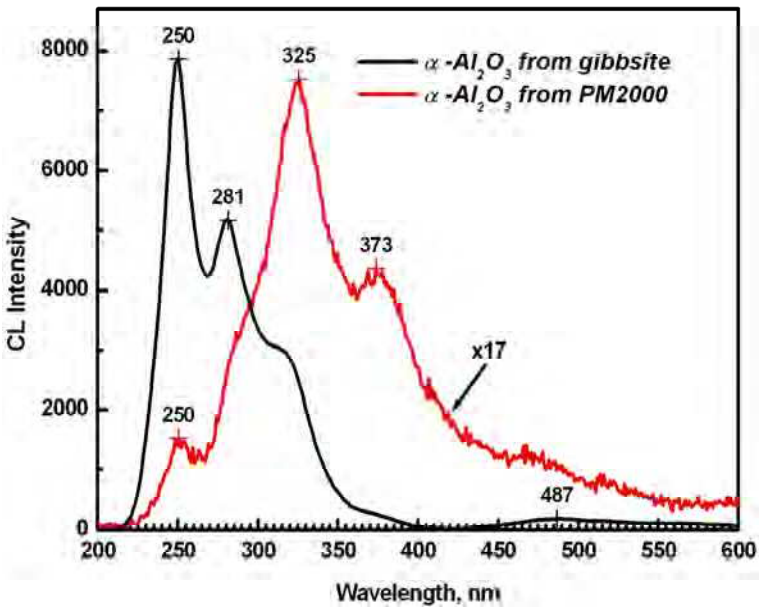

Fig. 9. CL spectra of α-Al_2O_3, formed by calcination of gibbsite powder at 1573 K for 24 h (black line) and by oxidation of PM2000 at 1223K for 72h (red line), obtained in the region of 200 to 600 nm at room temperature.

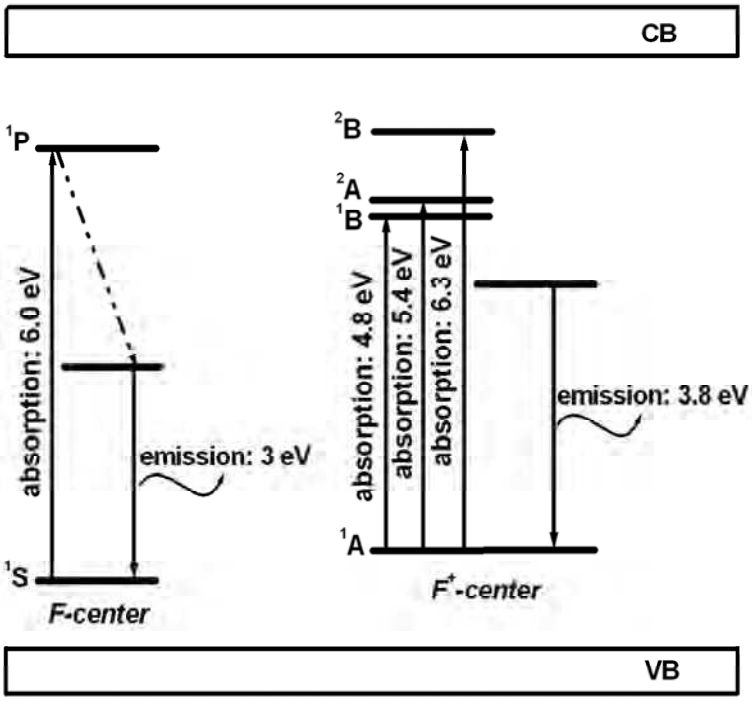

Fig. 10. Schematic energy level diagram for absorption and emission of F- and F^+-centres in α-Al_2O_3 crystal.

In Ref. (Evans, 1994), synthetic sapphire single crystals grown by four different techniques all showed an anisotropic 5.4 eV (230 nm) absorption broad band. There was not any other absorption band presented in his cases. As for the nanometer-sized Al_2O_3 powder apart from normal lattice vacancy-type defects such as the F-, F^+- and F_2-type centers it also has the surface defect because the nanometer powder has a larger specific surface area and there exists a lot of dangling bonds in the surface.

Experimental measurements of absorption and luminescence energies for single-vacancy and for dimer centers in Al_2O_3 are collected in Table 5.

	Absorption	Luminescence
F center	6.0	3.00
F^+ center	6.3, 5.4, 4.8	3.80
F_2	4.1	2.40
F_2^+	3.5	3.26
F_2^{2+}	2.7	2.22

Table 5. Experimental measurements of optical properties for single-vacancy and for dimer centers in Al_2O_3, energies are in eV (Crawford, 1984; Evans et al., 1994).

The band of F-centers is absent in both samples due to the existence of impurity Cr (Aoki, 1996). For instance, the CL intensity at 3.81 eV (F^+-center) of the α-Al_2O_3 formed from gibbsite is approximately 5 times higher than that of the α-Al_2O_3 formed from PM2000 measured under the same excitation conditions. The main specific feature of the CL spectra of the α-Al_2O_3 is the presence of a new emission band with the maximum at 3.32 eV. It is a possible that the new emission band is related to surface F_s-centers concentrating on nanoparticle boundaries (Evans, 1995).

Luminescence spectra obtained for anion-deficient aluminum corundum exposed to different types of excitation and stimulation exhibit luminescence with nanosecond (F^+-centers), microsecond (Ti^{3+} and Al^+_i) and millisecond (F and Cr^{3+}) decay times (Surdo et al., 2005). Significantly, the aforementioned centers, which actively participate in relaxation processes, have considerably different decay times t and emission band maxima $h\nu$ (Table 6).

Parameter	F^+	F	Al_i^+	Cr^{3+}	Ti^{3+}
$h\nu$ (eV)	3.8	3.0	2.4	1.79	1.75
τ	2 ns	34 ms	56 μs	4 ms	3.5 μs

Table 6. Basic parameters of the emission of most active centers (Surdo et al., 2001; Springis & Valbis, 1984)

The band 487 nm (2.54 eV) can be related to the aggregate F_2-centers produced by double-oxygen vacancies and the centers formed by interstitial aluminum ions. It is known that these centers are responsible for the green luminescence in highly disordered crystals of aluminum oxide (Tale et al., 1996; Springis & Valbis, 1984).

3.3.2 Cr^{3+} in Al_2O_3

A classic example of the isolated luminescent centre is Cr^{3+} in Al_2O_3 (ruby) when the excited electronic energy levels of the host are at much higher energy than those of the dopant ion. The dopant ion colours the colourless host lattice red. If the concentration of the dopant ion is low, the interaction between the dopant ions can be neglected. This is what we consider here as an isolated luminescent centre.

Different impurities in corundum (α-Al_2O_3) produce different color varieties. All colors of corundum are referred to as sapphire, except for the red color, which is known as ruby. Corundum has a trigonal lattice D^6_{3d} structure. The crystals have an approximately hexagonal closed packing structure of oxygen and metal atoms. The six oxygen ions are octahedrally coordinated cations; and only two-thirds of the octahedral sites are filled. If corundum has more than 1000 ppm Cr^{3+} ions as impurities, it is referred to as a ruby. Rubies can be used in solid-state lasers (Soukieh et al., 2004), and they fetch high prices in gem markets. Chromium can be substituted for the aluminum in corundum and is present as chromium oxide. The Cr^{3+} ion is slightly larger than Al^{3+}; therefore, it naturally enters easily into the corundum structure. As a result, Cr^{3+} ions form $3d^3$, with only three unpaired electrons in the 3d orbitals. If the Cr^{3+} ion is located in the Al^{3+} site in corundum, it coordinates the six oxygens into a distorted octahedral configuration (Nassau, 1983).

According to the ligand field theory (Figgis et al., 2000), splitting of the $3d^3$ (Cr^{3+}) orbital should result in the spectroscopic terms $^4A_2$ (*A*: no degeneracy) , $^4T_2$, $^4T_1$ (*T*: three fold degeneracy), and ^2E (*E*: two fold degeneracy).

For Cr^{3+} in Al_2O_3 crystal, Cr^{3+} substitutes for some of Al^{3+}, and adopts octahedral ligand coordination. The 3d levels are extremely host sensitive. The strong crystal field in Al_2O_3 leads to the splitting of 3d electron orbits of Cr^{3+} and produces the ground level: $^4A_2$, and the excited states: ^2E, $^4T_2$, and $^4T_1$, etc. the transitions from $^4A_2$ to $^4T_2$, and $^4T_1$ are spin-allowed, so these energy levels act as broad pumping levels. The ^2E is the narrow lowest excited band, acting as emitting level. The unusual magnitude of this crystal field splitting extends the lowest ^2E state 14400 cm^{-1} (694 nm) above the ground state. Thus the ^2E-$^4A_2$ transition of Cr^{3+}: Al_2O_3 crystal lies in visible spectral region. Exciting any of the pumping bands of $^4T_2$, and $^4T_1$ results in fast relaxation to lowest ^2E excited state. At room temperature, the fluorescence emitting from ^2E state appears as a sharp band with a peak at 694 nm corresponding to the transition to the ^2E terminal state. The Cr^{3+} ion has two strong absorption bands in the visible part of the spectrum, which explain the red color, i.e., 2.2 eV light can be absorbed to raise the chromium from the $^4A_2$ ground level to the $^4T_2$ excited level as absorption in the yellow-green, and 3.0 eV light raises it to the $^4T_1$ level as violet absorption. In addition, the absorption decreases to zero in the red region below 2.0 eV. Therefore, rubies have a red color with a slight purple overtone.

Chromium impurity in α-Al_2O_3 lattice is characterised by two bands of absorption (3.1 and 2.2 eV) and one fine emission structure peaked at 1.8 eV (693 nm) as summarised in Fig. 11.

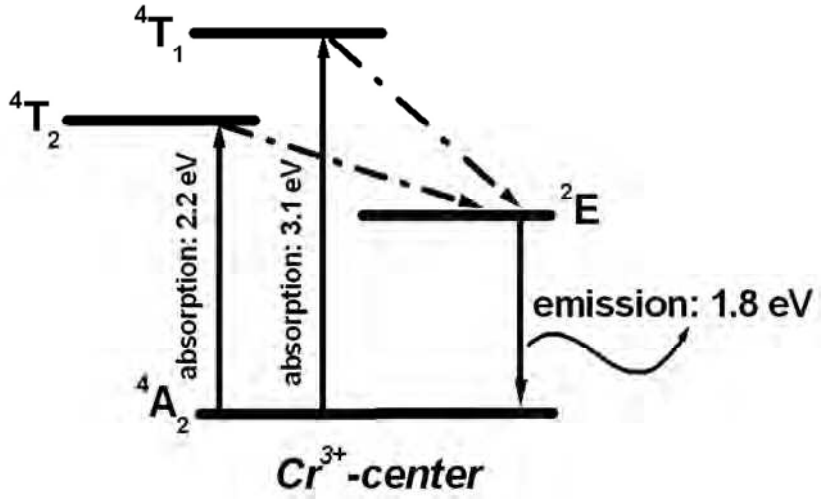

Fig. 11. Schematic energy level diagram for absorption and emission of Cr^{3+}-center in α-Al_2O_3 crystal.

In oxide insulators, a number of transition metal and rare earth impurities act as luminescence centers. The trivalent chromium ion (Cr^{3+}), with electronic configuration $3d^3$, is an efficient luminescence center in many light-metal oxides, including Al_2O_3 and MgO. The trivalent chromium ion enters substitutionally and is surrounded by an octahedron of oxygen ions. In aluminum oxide, the surroundings of the chromium ion are not quite cubic, as the oxygen octahedron is stretched along its trigonal symmetry axis C_3.

Chromium in α-Al_2O_3 lattice gives a luminescence in the visible domain. In CL, the narrow band at 693 nm is attributed to chromium impurity (Ghamnia et al., 2003). In Al_2O_3:Cr^{3+} (ruby) the apparent lifetime of the R-line emission may increase from the intrinsic value of 3.8 ms up to 12 ms (Auzel & Baldacchini, 2007).

The typical CL spectra of α-Al_2O_3, formed by calcination of gibbsite powder at 1573 K for 24 h (black line) and by oxidation of PM2000 at 1223K for 72h (red line), obtained in the region of 600 to 800 nm at room temperature are shown in Fig. 12. The sharp band at 693 nm (1.79 eV), with a radiative lifetime τ_R~4 ms (de Wijn, 2007), as well as features at 706 nm (1.76 eV) and 713 nm (1.74 eV) undoubtedly belongs to Cr^{3+} emission in α-alumina, and the subband at 677 nm (1.83 eV) is attributed to the ^2E–$^4A_2$ transition of Mn^{4+} ions in Al_2O_3 (Jovanic, 1997; Geschwind et al., 1962; Crozier, 1965).

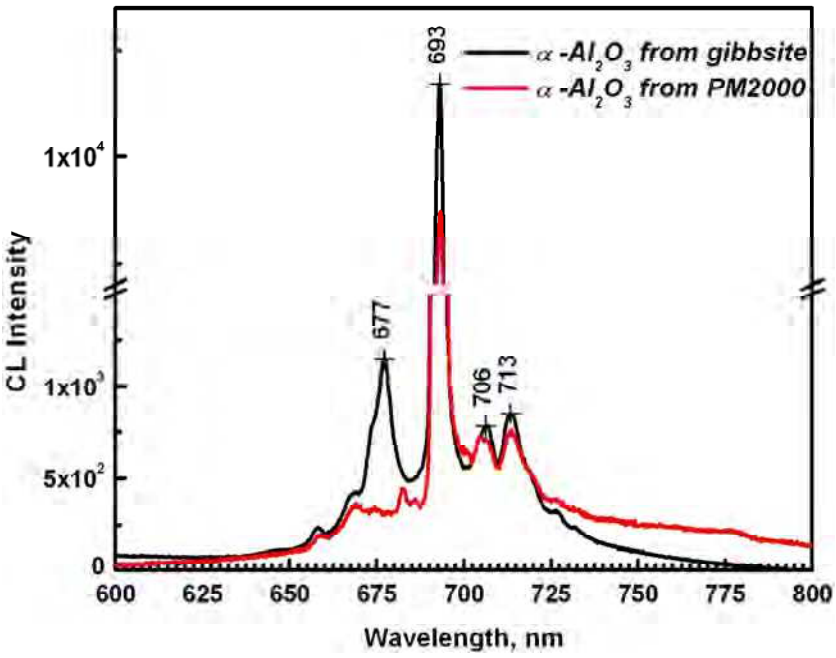

Fig. 12. CL spectra of α-Al_2O_3, formed by calcination of gibbsite powder at 1573 K for 24 h (black line) and by oxidation of PM2000 at 1223K for 72h (red line), obtained in the region of 600 to 800 nm at room temperature.

Mn^{4+} is known to emit doublet lines at 672 and 676 nm in α-Al_2O_3 (Kulinkin et al., 2000).

A similar emission was recently reported in α-Al_2O_3 microcones (Li et al., 2010). Thus, it can be concluded that the incorporation of Mn^{4+} ions in α-Al_2O_3 observed in the experiment is irreversible and occurs during its formation from the Mn^{4+} ions dissolved quite uniformly in the bulk of the low-temperature polymorphic modifications of alumina (gibbsite →χ-→κ-→α-Al_2O_3). The Mn^{4+} impurity emission at 677 nm is absent in α-alumina films obtained by oxidation of a metallic FeCrAl alloy. Taking into account high sensitivity of the method, this indicates very low concentration of such ions.

4. Conclusion

α–Al_2O_3 was prepared either by calcination of gibbsite and also generated by oxidation of a metallic FeCrAl alloy. The Mn^{4+} impurity emission at 1.83 eV is absent in α-alumina thin films obtained by oxidation of a metallic FeCrAl alloy. The band of F-centers is absent in both samples due to the existence of impurity Cr. The difference in oxygen vacancies (F^+-centers) amount between α–Al_2O_3 from gibbsite and from PM2000 was confirmed by CL spectra.

5. References

Aoki, Y.; My, N. T.; Yamamoto, S. & Naramoto, H. (1996). Luminescence of sapphire and ruby induced by He and Ar ion irradiation. *Nuclear Instruments and Methods in Physics Research Section B*, Vol.114, No.3-4, (July 1996), pp. 276-280, ISSN 0168-583X

Auzel, F. & Baldacchini, G. (2007). Photon trapping in ruby and lanthanide-doped materials: Recollections and revival. *Journal of Luminescence*, Vol.125, No.1-2, (July-August 2007), pp. 25-30, ISSN 0022-2313

Barker, Jr, A.S. (1963). Infrared lattice vibrations and dielectric dispersion in corundum. *Physical Review*, Vol.132, No.4, (November 1963), pp. 1474–1481, ISSN 0031-899X

Boumaza, A. & Djelloul, A. (2010). Estimation of the intrinsic stresses in a-alumina in relation with its elaboration mode. *Journal of Solid State Chemistry*, Vol.183, No.5, (May 2010), pp. 1063–1070, ISSN 0022-4596

Boumaza, A.; Djelloul, A. & Guerrab, F. (2010). Specific signatures of α-alumina powders prepared by calcination of boehmite or gibbsite. *Powder Technology*, Vol.201, No.2, (July 2010), pp. 177–180, ISSN 0032-5910

Brewer, J.D.; Jeffries, B.T. & Summers, G.P. (1980). Low-temperature fluorescence in sapphire. *Physical Review B condensed matter and Materials Physics* Vol.22, No.10, (November 1980), pp. 4900–4906, ISSN 1098-0121

Brindley, G.W. & Choe, J.O. (1961). Reaction series gibbsite→chi alumina→kappa alumina→corundum. *American Mineralogist*, Vol.46, No.7-8, (July-August 1961), pp. 771-785, ISSN 0003-004X

Crawford Jr., J.H. (1984). Defects and defect processes in ionic oxides: Where do we stand today?. *Nuclear Instruments and Methods in Physics Research Section B*, Vol.1, No.2-3, (February 1984), pp. 159-165, ISSN 0168-583X

Crozier, M.H. (1962). Optical Zeeman effect in the R_1 and R_2 lines of Mn^{4+} in Al_2O_3. *Physics Letters*, Vol.18, No.3, (September 1965), pp. 219-220, ISSN 0031-9163

de Wijn, H.W. (2007). Phonon physics in ruby studied by optical pumping and luminescence. *Journal of Luminescence*, Vol.125, No.1-2, (July-August 2007), pp. 55-59, ISSN 0022-2313

Evans, B.D.; Pogatshnik, G.J. & Chen, Y. (1994). Optical properties of lattice defects in α-Al_2O_3. *Nuclear Instruments and Methods in Physics Research Section B*, Vol.91, No.1-4, (June 1994), pp. 258-262, ISSN 0168-583X

Evans, B.D. (1994). Ubiquitous blue luminescence from undoped synthetic sapphires. *Journal of Luminescence*. Vol.60-61, (April 1994), pp. 620-626, ISSN 0022-2313

Evans, B.D. (1995). A review of the optical properties of anion lattice vacancies, and electrical conduction in α-Al_2O_3: their relation to radiation-induced electrical degradation. *Journal of Nuclear Materials*, Vol.219, (March 1995), pp. 202-223, ISSN 0022-3115

Figgis, B.N. & Hitchman, M.A. (2000). *Ligand Field Theory and its Applications*, John Wiley & Sons Inc, ISBN 978-0-471-31776-0, New York

Geschwind, S.; Kisliuk, P.; Klein, M.P.; Remeika, J.P. & Wood, D.L. (1962). Sharp-Line Fluorescence, Electron Paramagnetic Resonance, and Thermoluminescence of Mn^{4+} in *a*-Al_2O_3. *Physical Review*, Vol.126, No.5, (June 1962), pp. 1684-1686, ISSN 0031-899X

Ghamdi, A. Al. & Townsend, P.D. (1990). Ion beam excited luminescence of sapphire. *Nuclear Instruments and Methods in Physics Research B*, Vol.46, No.1-4, (February 1990), pp. 133-136, ISSN 0168-583X

Ghamnia, M.; Jardin, C. & Bouslama, M. (2003). Luminescent centres F and F^+ in α-alumina detected by cathodoluminescence technique. *Journal of Electron Spectroscopy and Related Phenomena*, Vol.133, No.1-3, (November 2003), pp. 55-63, ISSN 0368-2048

Golightly, F.A.; Stott, F.H. & Wood, G.C. (1979). The Relationship Between Oxide Grain Morphology and Growth Mechanisms for Fe-Cr-Al and Fe-Cr-Al-Y Alloys. *Journal of The Electrochemical Society*, Vol.126, No.6, (June 1979), pp. 1035-1042, ISSN 0013-4651

Hou, P.Y.; Zhang, X.F. & Cannon, R.M. (2004). Impurity distribution in Al_2O_3 formed on an FeCrAl alloy. *Scripta Materialia*, Vol.50, No.1, (January 2004) pp. 45–49, ISSN 1359-6462

http://accuratus.com/alumox.html/ Aluminum Oxide, Al_2O_3 Material Characteristics

Jheeta, K.S.; Jain, D.C.; Fouran Singh; Ravi Kumar & Garg, K.B. (2006). Photoluminescence and UV–vis studies of pre- and post-irradiated sapphire with 200 MeV Ag^{8+} ions. *Nuclear Instruments and Methods in Physics Research B*, Vol.244, No.1, (March 2006), pp. 187–189, ISSN 0168-583X(02)

Jovanic, B.R. (1997). Shift under pressure of the luminescence transitions of corundum doped with Mn^{4+}. *Journal of Luminescence*, Vol.75, No.2, (September 1997), pp. 171-174, ISSN 0022-2313

Kislov, A.N.; Mazurenko, V.G.; Korzov, K.N. & Kortov, V.S. (2004). Interionic potentials and localized vibrations in Al_2O_3 crystals with vacancies. *Physica B: Condensed Matter,* Vol.352, No.1-4, (October 2004), pp. 172–178, ISSN 0921-4526

Kogure, T. (1999). Dehydration sequence of gibbsite by electron beam irradiation in a TEM. *Journal of the American Ceramic Society*, Vol. 82, No.3, (March 1999), pp. 716-720, ISSN 0002-7820

Kortov, V.S.; Ermakov, A.E.; Zatsepin, A.F. & Nikiforov, S.V. (2008). Luminescence properties of nanostructured alumina ceramic. *Radiation Measurements*, Vol.43, No.2-6, (February-June 2008), pp. 341-344, ISSN 1350-4487

Kortov, V. & Milman, I. (1996). Some New Data on Thermoluminescence Properties of Dosimetric Alpha-Al_20_3 Crystals. *Radiation Protection Dosimetry*, Vol.65, No.1-4, (June 1996), pp. 179-184, ISSN 0144-8420

Kulinkin, A. B.; Feofilov, S. P. & Zakharchenya, R. I. (2000). Luminescence of impurity 3*d* and 4*f* metal ions in different crystalline forms of Al_2O_3. *Physics of the Solid State*, Vol.42, No.5, (May 2000), pp. 857-860, ISSN 1063-7834

La, S.; Bartram, R.H. & Cox, R.T. (1973). The F^+ center in reactor-irradiated aluminum oxide . *Journal of Physics and Chemistry of Solids*, Vol.34, No.6, (June 1973), pp. 1079-1086, ISSN 0022-3697

Li, P.G.; Lei, M. & Tang, W.H. (2010). Raman and photoluminescence properties of α-Al_2O_3 microcones with hierarchical and repetitive superstructure. *Materials Letters*, Vol.64, No.2, (January 2010), pp. 161-163, ISSN 0167-577X

Ma, C.; Chang, Y.; Ye, W.; Shang, W. & Wang, C. (2008). Supercritical preparation of hexagonal γ-alumina nanosheets and its electrocatalytic properties. *Journal of Colloid and Interface Science*, Vol.317, No.1, (January 2008), pp. 148–154, ISSN 0021-9797

MacKenzie, K.J.D.; Temuujin, J. & Okada, K. (1999). Thermal decomposition of mechanically activated gibbsite. *Thermochimica Acta*, Vol.327, No.1-2, (March 1999), pp. 103–108, ISSN 0040-6031

Mennicke, C.; Schumann, E.; Ruhle, M.; Hussey, R.J.; Sproule, G.I. & Graham, M.J. (1998). The Effect of Yttrium on the Growth Process and Microstructure of α-Al_2O_3 on FeCrAl. *Oxidation of metals*, Vol.49, No.5-6, (June 1998), pp. 455-466, ISSN 0030-770X

Michizono, S.; Saito, Y.; Suharyanto; Yamano, Y. & Kobayashi, S. (2007). Surface characteristics and electrical breakdown of alumina materials. *Vacuum*, Vol.81, No.6, (February 2007), pp. 762–765, ISSN 0042-207X

Monteiro, T.; Boemare, C.; Soares, M.J.; Alves, E.; Marques, C.; McHargue, C.; Ononye, L.C. & Allard, L.F. (2002). Luminescence and structural studies of iron implanted α-Al_2O_3. *Nuclear Instruments and Methods in Physics Research Section B: Beam Interactions with Materials and Atoms*, Vol.191, No.1-4, (May 2002), pp. 638-643, ISSN 0168-583(2)

Nassau, K. (1983). *The Physics and Chemistry of Color: The Fifteen Causes of Color,* John Wiley & Sons Inc, ISBN 0471867764, NewYork

Ollivier, B.; Retoux, R.; Lacorre, P.; Massiot, D. & Férey, G. (1997). Crystal Structure of Kappa Alumina an X-Ray powder diffraction, TEM and NMR study. *Journal of Materials Chemistry*, Vol.7, No.6, (1997), pp. 1049– 1056, ISSN 0959-9428

Oster, L.; Weise, D. & Kristiapoller, N. (1994). A study of photostimulated thermoluminescence in C-doped alpha -Al_2O_3 crystals. *Journal of Physics D: Applied Physics*, Vol.27, No.8, (August 1994), pp. 1732-1736, ISSN 0022-3727

Przybylski, K.; Garrett-Reed, A.J.; Pint, B.A.; Katz, E.P. & Yurek, G.J. (1987). Segregation of Y to Grain Boundaries in the Al_2O_3 Scale Formed on an ODS Alloy. *Journal of The Electrochemical Society*, Vol.134, No.12, (December 1987), pp. 3207-3208, ISSN 0013-4651

Quadakkers, W.J.; Elschner, A.; Speier, W. & Nickel, H. (1991). Composition and growth mechanisms of alumina scales on FeCrAl-based alloys determined by SNMS. *Applied Surface Science*, Vol.52, No.4, (December 1991), pp. 271-287, ISSN 0169-4332

Rodríguez-Carvajal, J. (1993). Recent Advances in Magnetic Structure Determination by Neutron Powder Diffraction. *Physica B Condensed Matter*, Vol. 192, No. *1-2*, (October 1993), pp. 55–69, ISSN 0921-4526

Saalfeld, H. & Wedde, M. (1974). Refinement of the structure of gibbsite, Al(OH)3. *Zeitschrift für Kristallographie*, Vol.139, No.1-2, (April 1974), pp. 129–135, ISSN 0044-2968

Saalfeld, H.N. (1960). Strukturen des Hydrargillitis und der Zwis- chenstufen biem Entwassern. *Neues Jahrbuch für Mineralogie,* Vol.95, No.7-8, (1960), pp. 1–87, ISSN 0077-7757

Soukieh, M.; Ghani, B.A. & Hammadi, M. (2004). Numerical calculations of intracavity dye Q-switched ruby laser. *Optics and Lasers in Engineering*, Vol.41, No.1, (January 2004), pp. 177-187, ISSN 0143-8166

Springis, M.J. & Valbis, J.A. (1984). Visible luminescence of colour centres in sapphire. *Physica status solidi. B*, Vol.123, No.1, (May 1984), pp. 335-343, ISSN 0370-1972

Stumpf, H.C.; Russel, A.S.; Newsome, J.W. & Tucker, C.M. (1950). Thermal transformations aluminas and alumina hydrates - Reaction with 44% Technical Acid, *Industrial & Engineering Chemistry Research*, Vol.42, No.7, (July 1950), pp. 1398-1403, ISSN 0888-5885

Surdo, A.I.; Kortov, V.S. & Pustovarov, V.A (2001). Luminescence of F and F^+ centers in corundum upon excitation in the interval from 4 to *40* eV. *Radiation Measurements*, Vol.33, No.5, (October 2001), pp. 587-591, ISSN 1350-4487

Surdo, A.I.; Pustovarov, V.A.; Kortov, V.S.; Kishka, A.S. & Zinin, E.I. (2005). Luminescence in anion-defective α-Al_2O_3 crystals over the nano-, micro- and millisecond intervals. *Nuclear Instruments and Methods in Physics Research A*, Vol.543, No.1, (May 2005), pp. 234–238, ISSN 0168-9002

Tale, I.; Piters, T.M.; Barboza-Flores, M.; Perez-Salas, R.; Aceves, R. & Springis, M. (1996). Optical Properties of Complex Anion Vacancy Centres and Photo-Excited Electronic Processes in Anion Defective Alpha-Al_2O_3. *Radiation Protection Dosimetry*, Vol.65, No.1-4, (June 1996), pp. 235-238, ISSN 0144-8420

Whittington, B. & Ilievski, D. (2004). Determination of the gibbsite dehydration reaction pathway at conditions relevant to Bayer refineries. *Chemical Engineering Journal*, Vol.98, No.1-2, (March 2004), pp. 89-97, ISSN 1385-8947

Wood, G. C. (1970). High-temperature oxidation of alloys. *Oxidation of Metals*, Vol.2, No.1, (March 1970), pp. 11-57, ISSN 0030-770X

Yu, Z.Q.; Li, C. & Zhang, N. (2002). Size dependence of the luminescence spectra of nanocrystal alumina. *Journal of Luminescence*. Vol.99, No.1, (August 2002), pp. 29-34, ISSN 0022-2313

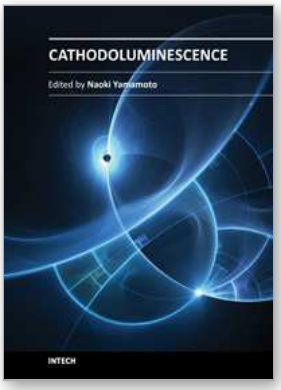

Cathodoluminescence

Edited by Dr. Naoki Yamamoto

ISBN 978-953-51-0362-2
Hard cover, 324 pages
Publisher InTech
Published online 28, March, 2012
Published in print edition March, 2012

Cathodoluminescence (CL) is a non-destructive technique to characterize optical and electronic properties of nanostructures in many kinds of materials. Major subject is to investigate basic parameters in semiconductors, impurities in oxides and phase determination of minerals. CL gives information on carrier concentration, diffusion length and life time of minority carriers in semiconductors, and impurity concentration and phase composition in composite materials. This book involves 13 chapters to present the basics in the CL technique and applications to particles, thin films and nanostructures in semiconductors, oxides and minerals. The chapters covered in this book include recent development of CL technique and applications to wide range of materials used in modern material science.

How to reference

In order to correctly reference this scholarly work, feel free to copy and paste the following:

Djelloul Abdelkader and Boumaza Abdecharif (2012). Peculiarity of the Cathodoluminescence of Ipha- Alumina Prepared by Calcination of Gibbsite Powder or Generated by Oxidation of a Metallic FeCrAl Alloy, Cathodoluminescence, Dr. Naoki Yamamoto (Ed.), ISBN: 978-953-51-0362-2, InTech, Available from: http://www.intechopen.com/books/cathodoluminescence/peculiarity-of-the-cathodoluminescence-of-alumina-prepared-by-calcination-of-gibbsite-powder-or-gene

INTECH
open science | open minds

InTech Europe
University Campus STeP Ri
Slavka Krautzeka 83/A
51000 Rijeka, Croatia
Phone: +385 (51) 770 447
Fax: +385 (51) 686 166
www.intechopen.com

InTech China
Unit 405, Office Block, Hotel Equatorial Shanghai
No.65, Yan An Road (West), Shanghai, 200040, China
中国上海市延安西路65号上海国际贵都大饭店办公楼405单元
Phone: +86-21-62489820
Fax: +86-21-62489821